JOURNAL OF NEUROTRAUMA 32:1020–1029 (July 1, 2015)
© Mary Ann Liebert, Inc.
DOI: 10.1089/neu.2014.3677

A Threshold Shear Force for Calcium Influx in an Astrocyte Model of Traumatic Brain Injury

Mohammad Mehdi Maneshi,[1] Frederick Sachs,[2] and Susan Z. Hua[1,2]

Abstract

Traumatic brain injury (TBI) refers to brain damage resulting from external mechanical force, such as a blast or crash. Our current understanding of TBI is derived mainly from *in vivo* studies that show measurable biological effects on neurons sampled after TBI. Little is known about the early responses of brain cells during stimuli and which features of the stimulus are most critical to cell injury. We generated defined shear stress in a microfluidic chamber using a fast pressure servo and examined the intracellular Ca^{2+} levels in cultured adult astrocytes. Shear stress increased intracellular Ca^{2+} depending on the magnitude, duration, and rise time of the stimulus. Square pulses with a fast rise time ($\sim$2 ms) caused transient increases in intracellular Ca^{2+}, but when the rise time was extended to 20 ms, the response was much less. The threshold for a response is a matrix of multiple parameters. Cells can integrate the effect of shear force from repeated challenges: A pulse train of 10 narrow pulses (11.5 dyn/cm^2 and 10 ms wide) resulted in a 4-fold increase in Ca^{2+} relative to a single pulse of the same amplitude 100 ms wide. The Ca^{2+} increase was eliminated in Ca^{2+}-free media, but was observed after depleting the intracellular Ca^{2+} stores with thapsigargin suggesting the need for a Ca^{2+} influx. The Ca^{2+} influx was inhibited by extracellular Gd^{3+}, a nonspecific inhibitor of mechanosensitive ion channels, but it was not affected by the more specific inhibitor, GsMTx4. The voltage-gated channel blockers, nifedipine, diltiazem, and verapamil, were also ineffective. The data show that the mechanically induced Ca^{2+} influx commonly associated with neuron models for TBI is also present in astrocytes, and there is a viscoelastic/plastic coupling of shear stress to the Ca^{2+} influx. The site of Ca^{2+} influx has yet to be determined.

Key words: blast; intracellular Ca^{2+}; mechanosensitive ion channel (MSC); shear stress; traumatic brain injury (TBI)

Introduction

Traumatic brain injury (TBI) results from an external mechanical force, such as a blast or crash. Traumatic injury is normally classified as a focal injury that results in cerebral contusions at a specific location or diffuse axonal injury over a widespread area, probably resulting from shear forces.[1–4] The deformation caused by the shear forces in diffuse TBI is difficult to define because it occurs throughout the brain and is often mixed with secondary injuries resulting from subsequent biochemical and metabolic dysfunction.[5,6] Most TBI patients exhibit mild or minimal observable damage upon the initial shock. However, even low-amplitude shear forces may induce biochemical processes that yield serious pathology hours and days later.[7–9] To better understand the development of damage, we began an analysis of the primary causes of cellular responses to shear forces by using high-speed stimuli to establish causality.

Astrocytes are the most abundant cells in the brain and provide a critical link between the circulatory system and the maintenance of neurons (tripartite synapses, neurotransmitter processing, and so on).[10] Although astrocytes have been considered less susceptible to injury than neurons, they can transmit mechanical forces to neurons and accept forces from them during TBI. Astrocytes can propagate damage signals through Ca^{2+} waves, signal to neurons through neurotransmitters, and alter ion concentrations in the extracellular space.[10–12] Significantly, astrocyte death precedes neuronal death during TBI.[13]

The earliest measurable reaction of astrocytes to traumatic injury is elevation of intracellular Ca^{2+}. Because astrocytes have cationic mechanosensitive ion channels (MSCs) that are permeable to Ca^{2+},[12,14,15] mechanical stimuli (stretching or shear forces) can activate them and cause an increase in intracellular Ca^{2+}.[16] However, most studies have been conducted by stretching flexible substrates with adherent cultured cells[17–19] or with fluid shear forces that are much slower than the shockwaves that produce TBI.[18,20] Little is known about the coupling of intracellular Ca^{2+} responses to blast-like shear force in astrocytes.

A cell's response to mechanical insults is nonlinear, so the nature of the mechanical stimulus plays a crucial role in subsequent pathology.[3,21,22] Using a blast chamber to apply rapid pressure and

[1]Department of Mechanical and Aerospace Engineering and [2]Department of Physiology and Biophysics, SUNY-Buffalo, Buffalo, New York.

shear forces to cell cultures, Raven and colleagues showed that intracellular Ca^{2+} is more responsive to shear than to changes in pressure.[23] Further, traumatic cell injury depends not only on the intensity of the loading, but also on the loading rate.[24,25] Rapid shear deformations increase the membrane permeability to small dye molecules and also decrease cell viability.[24] These studies suggest that cascades of cell responses are governed by multiple parameters.

In this work, we defined thresholds with multiple input parameters, including intensity, rise time, duration, duty cycle, and so on. We used tissue-cultured adult astrocytes in a microfluidic chamber where shear stress was controlled by a fast pressure servo,[26] generating shear forces of known waveform while we measured the intracellular Ca^{2+} response. Pulsed shear with fast rise times ($\sim$2 ms) were more effective than pulses with slower rise times defining the presence of an effective viscosity. Nonlinear summation was visible by the response of cells to repeated subthreshold stimuli. The multi-dimensional thresholds are summarized with a mathematical model. Using different pharmacological inhibitors, we found that the intracellular Ca^{2+} elevation involves influx pathways that do not include GsMTx4-sensitive MSCs or voltage-sensitive calcium channels.

Methods

Flow chamber and pressure servo pump

The microfluidic flow chamber is a parallel-plate flow system made of a 25-mm diameter cover-glass substrate and a 1-mm-thick glass slide separated by polydimethylsiloxane (PDMS) walls (Fig. 1A). The chamber dimensions were 1000 μm wide, 15 mm long, and 100 μm high. The device was fabricated using soft lithography following the fabrication process described previously.[27] For inlet and outlet, holes were punched through the PDMS at the ends of the chamber. The chip was mounted on a home-made assembly that allowed fluorescence imaging. The chamber substrate was coated with human fibronectin (BD Biosciences, San Jose, CA) and rinsed 1 h before seeding the cells.

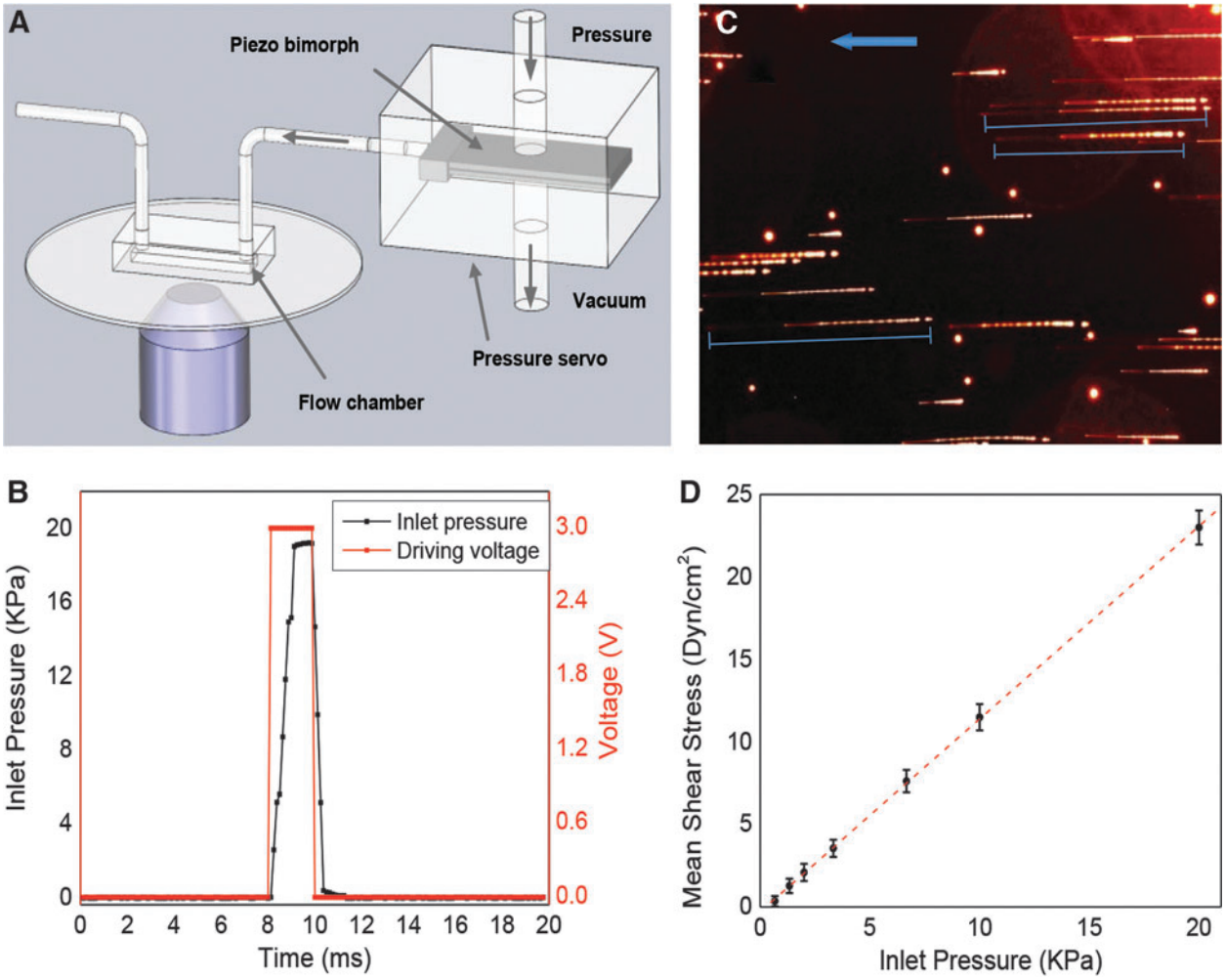

FIG. 1. Calibration of shear stress in microfluidic chamber. (**A**) Schematic of experimental setup. High-speed pressure servo was connected to a microfluidic chamber to generate controlled fluid shear stimuli. (**B**) Comparison of triggering voltage pulse (red) and pressure rise (black) at inlet of the chamber, showing a rise time of 1 ms can be achieved. (**C**) Trajectory of microbeads under a flow pulse of 6.5 kPa for 10 ms. The image was collected from the middle plane of the chamber, $\sim$50 μm from the bottom. Blue arrow indicates flow direction. (**D**) Dependence of average shear stress on inlet pressure. Maximum flow rate was estimated from the length of the streaks and shear stress calculated as described in Methods. Each data point was averaged from >8 streaks in each frame for a total of 10 frames of four experiments. Error bar indicates standard error of the mean. Color image is available online at www.liebertpub.com/neu

An ultra-fast piezo-driven pressure servo (ALA Scientific Instruments, Farmingdale, NY) was used to generate pressure pulses of known waveform with a time resolution of ~1 ms to drive the chamber.[26] The stimuli included steps and ramps and the pressure was monitored at the chamber inlet to parameterize the shear stress. To mimic blast waves in the fluids, the waveform was chosen to closely resemble a classic Friedlander curve.[28] Flow velocity was obtained experimentally by tracking fluorescent microbeads. Mean flow rate was estimated from the measured data following established theory.[29] The wall shear stress, τ, was calculated using the empirical equation, $\tau = 6\mu Q/wh^2$, where μ is the dynamic viscosity of the fluid, Q is the volume flow rate, and w and h are the width and the height of the chamber, respectively.[30] Viscosity was assumed to be 10^{-3} Pa s.

Cell culture

Primary adult astrocytes were isolated from gelatin-sponge implants from adult Sprague-Dawley rat brains provided by Dr. Thomas Langan (SUNY-Buffalo, Buffalo, NY). Astrocytes were maintained in Dulbecco's modified Eagle's medium, 10% fetal bovine serum, and 1% penicillin/streptomycin. Cells were transferred to the microfluidic chambers when the flasks reached 95% confluence and were cultured in the chamber for 3–5 days before the experiments. Media in the chamber were changed every 24 h to sustain the cell growth. To permit phenotypic maturation of astrocytes, they were only used in experiments between passages 4 and 12.[31]

Calcium dye loading and fluorescence imaging

Before the experiments, cells were gently washed with saline, followed by loading with the Ca^{2+}-sensitive dye, Fluo-4 AM (5 μM; Invitrogen, Carlsbad, CA), and kept in an incubator (37°C with 95% air and 5% CO_2) for 30 min. Chambers were then gently washed and returned to the incubator for ~8 min to allow cleavage of the dye molecules. Normal saline was used as the shearing fluid. Fluorescence images were acquired using an inverted microscope (Axiovert 200M; Carl Zeiss, Jena, Germany) equipped with a charge-coupled device (CCD) camera (AxioCam MRm; Carl Zeiss) and a 10× objective lens. The filter set (excitation [Ex], 470/40 nm; emission [Em], 525/50 nm) was used for Ca^{2+} imaging. Time-lapse images were obtained using software (AxioVision; Carl Ziess). To calibrate the shear stress in the microchannel produced by the pressure pulse, fluorescent microspheres (1 μm, Sulfate Fluospheres; Invitrogen) were dissolved in the saline. The trajectories of the sphere under different pressure pulses were acquired using the filter set (Ex, 580/25; Em, 605/70).

Solutions and reagents

Normal saline containing 1 mM of $CaCl_2$ was used as control solution. In Ca^{2+}-free solutions, $CaCl_2$ was replaced by $MgCl_2$. Gadolinium chloride (Sigma-Aldrich, St. Louis, MO) was freshly prepared as 10-mM stock solution in control solution before each experiment. Nifedipine, cis-diltiazem hydrochloride, and verapamil hydrochloride (Sigma-Aldrich) were each dissolved in ethanol and then diluted in saline to 10 μM (ethanol in the final solution was less than 1:1000). The enantiomer forms of GsMTx4 were made and purified according to previously published protocols.[32]

Statistical analysis

Relative Ca^{2+} intensity was calculated using $\frac{\Delta F}{F_0} = \frac{F - F_0}{F_0}$, where F and F_0 are the mean fluorescence intensities of selected cells at time t and t = 0, respectively. Background intensity was subtracted before the calculation. A new cell culture was used for each experiment. Mean calcium change was averaged over N selected cells from each image and over multiple experiments. The statistical analysis used the standard error of the mean. To summarize the multi-dimensional thresholds, the profile of peak Ca^{2+} intensity was fit with a two-state Boltzmann equation (Equation 1):

$$\frac{\Delta F}{F_{max}} = \frac{1}{1 + e^{(a*x^{-m}*y^{-n}+h)}} \quad (1)$$

where x and y are, respectively, the amplitude and duration of the shear pulse; a, m, n, and h are constants and were extracted from the fitting as $a = 32.55$, $m = 0.44$, $n = 0.096$, and $h = -6.54$. The fidelity of the fitting was measured by R^2, coefficient of determination, and $R^2 \geq 0.95$ for these fits.

Results

Shear stress calibration in flow chamber

We first calibrated the shear stress of various waveforms in the flow chamber without cells. Shear pulses of various amplitudes and durations were generated by the pressure servo connected to the flow chamber (Fig. 1A), and the pressure at the inlet of the chamber was measured using a pressure sensor. The pressure reached steady state value in ~1 ms when a square pulse was applied (Fig. 1B). To visualize the flow profile, fluorescent microspheres (1 μm) were dissolved in the solution. A series of pressure pulses were applied to generate a pulsatile fluid flow. The pulse width was set to be narrower than the camera shutter open time for each frame, so that the trajectory length (marked by blue lines in Fig. 1C) represents the total traveling distance of the beads during the pulse. Figure 1C shows a typical image of bead traces with a pressure pulse of 6.5 kPa and 10-ms duration. To minimize hydraulic effects of the chamber walls, the images were taken from the midplane of the chamber (focus plane, z = 50 μm) providing the maximum flow velocity. Note that there are two distinct segments along the streaks, a dimmer section (left end of the streak, Fig. 1C), representing the acceleration of the beads, and a brighter section (right end of the streak, Fig. 1C), representing the cruising and retraction. Each segment of the streaks was measured separately and the total length, averaged for all the beads in the field of view, was used to calculate maximum velocity in the chamber. The average velocity was estimated as half of the maximum velocity following the previous publication.[29] Shear stress in the chamber at each applied pressure is calculated from measured velocity and shown in Figure 1D, where each data point was averaged from 10 frames of four experiments. To verify the rise time, the time required to reach the steady-state shear stress, we applied a series of narrow pressure pulses with various rise times and measured the linearity of shear force to the pulse amplitude (Supplementary Materials S1) (see online supplementary material at http://www.liebertpub.com). The data show a limiting rise time of 2 ms defining the instrumental limit. The amplitude of the shear stress was directly proportional to the amplitude of the pressure when the pulse width was longer than this limit (Fig. 1D).

Ca^{2+} response depends on both magnitude and duration of the stimuli

To measure whether there is a threshold of the shear force, we measured the intracellular Ca^{2+} changes with narrow pulses of varying magnitudes and durations. Shockwaves from a blast typically generate pulsed shear forces of ~8-ms duration in the brain.[23] We first used stimuli of 10-ms pulse width, 2-ms rise time, and magnitudes ranging from 11.5 to 23 dyn/cm^2. Astrocytes responded to a shear of 23 dyn/cm^2 with a transient Ca^{2+} increase (Fig. 2A),

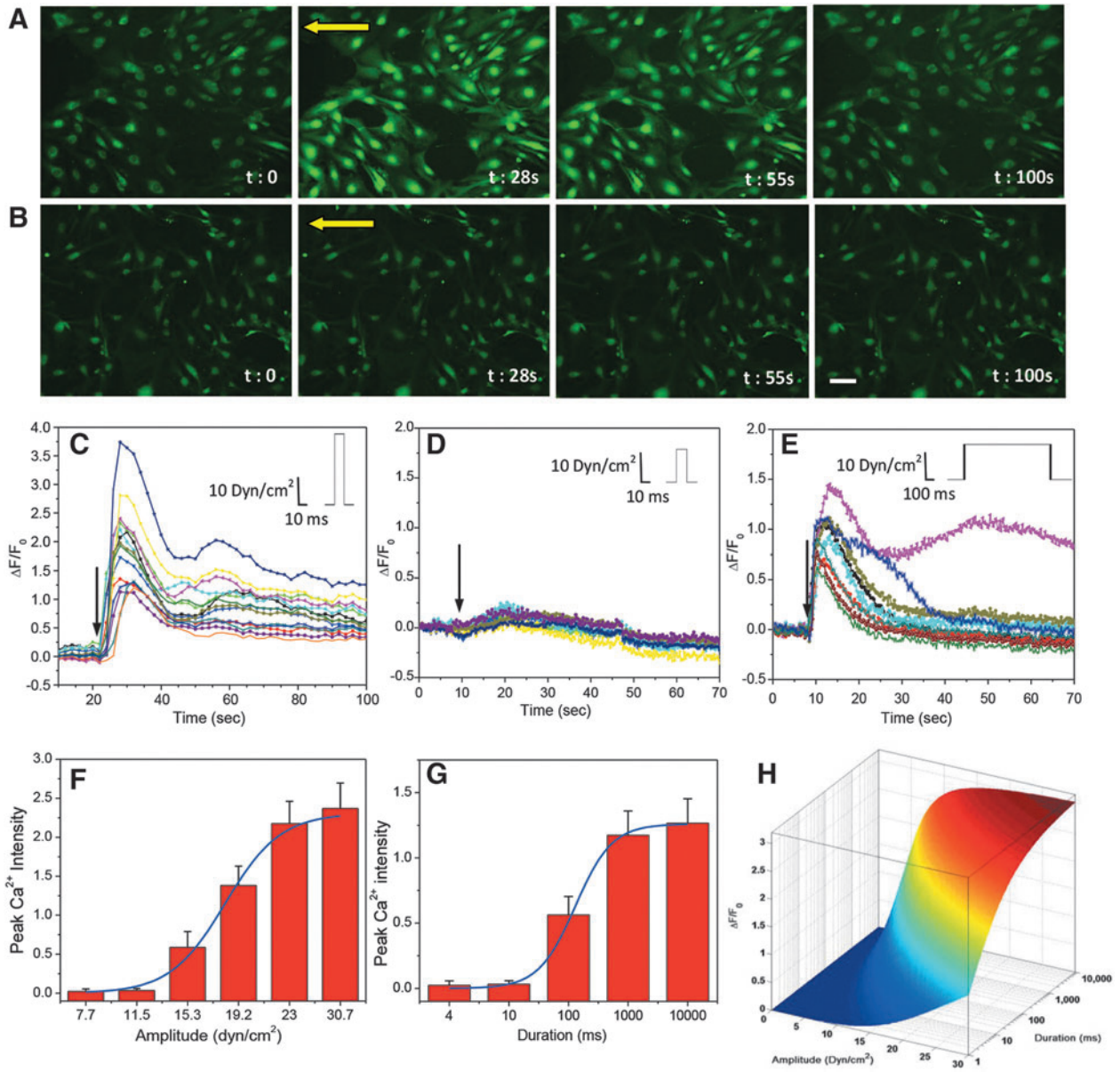

FIG. 2. Ca^{2+} response to shear pulses of different amplitudes and durations in astrocytes. (**A** and **B**) Fluorescence images of Fluo-4-loaded astrocytes subjected to a narrow shear pulse (10 ms duration and 2 ms rise time) of 23 (A) and 11.5 dyn/cm^2 (B). Yellow arrows indicate flow direction. (**C** and **D**) Time-dependent changes in Ca^{2+} intensity from selected cells in (A) and (B), respectively. (**E**) Ca^{2+} responses to a pulse of lower amplitude (11.5 dyn/cm^2), but with longer duration (1000 ms), showing that duration of the pulse affects the responses. (**F** and **G**) Statistics of peak Ca^{2+} intensity with pulses of different amplitude and duration ($n = 30$ for each condition) and corresponding fitting curves using Equation 1. (**H**) Profile of stimulus thresholds (amplitude and duration), showing the lowest threshold for Ca^{2+} response is 11.5 dyn/cm^2 for 10 ms. Scale bar represents 100 μm. Color image is available online at www.liebertpub.com/neu

but clearly did not respond to 11.5 dyn/cm^2 (Fig. 2B). The time course of changes in intracellular calcium concentration is shown in Figure 2C,D. The average peak change of cytosolic calcium was $\sim$250% at 23 dyn/cm^2 (Fig. 2C), compared with $\sim$5% at 11.5 dyn/cm^2 (Fig. 2D). Moreover, a large percentage of cells showed an instantaneous increase in calcium at the higher shear stresses (>95% at 23 dyn/cm^2), whereas a small percentage responded to low stress ($\sim$30% at 16 dyn/cm^2). Thus, there are significant variations in the mechanical responses and Ca^{2+} coupling properties of the cells, and averaging across cell populations is unwise given the nonlinearity. At longer times, some cells showed responses from calcium waves spreading from activated neighboring cells, and we excluded those cells. We tested six amplitudes and the peak Ca^{2+} levels suggested an effective threshold of $\sim$11.5 dyn/cm^2 (Fig. 2F). The molecular basis for the threshold is not known, but it may represent the force required to break some specific cytoskeletal bonds or the force required to open the Ca^{2+} influx channel.

Whereas the stimulus amplitude is a key parameter, the duration of the pulses also affects the response and together the two parameters establish a *multi*-dimensional threshold matrix for nominally square pulses. Working at a low amplitude of 11.5 dyn/cm^2, we examined response to longer pulses. At 10 ms, there was still no Ca^{2+} response (Fig. 2D). However, when the pulse width increased to 1000 ms, there was a clear increase in Ca^{2+} (Fig. 2E). The peak

Ca^{2+} level increased with duration, reaching a saturation at t = 1s (Fig. 2G). We used a two-state Boltzmann equation (Equation 1) to fit the profile of peak Ca^{2+} intensity, and the fitting curves are shown overlapped with the experimental data for various amplitudes (Fig. 2F) and durations (Fig. 2G). The fitting constants, $m = 0.44$ and $n = 0.096$, respectively, indicate the significance of amplitude and duration, showing that amplitude is the dominant parameter. The multi-dimensional threshold of both the amplitude and duration is shown in Figure 2H.

Ca^{2+} response is sensitive to shear loading rate

In neurons cultured in three-dimensional (3D) matrices, a rapid increase of strain resulted in rapid Ca^{2+} elevation and a decrease in viability, but there were no significant changes in Ca^{2+} for slow increases in strain,[25] suggesting an effective cellular viscosity. Using a similar *in vitro* model, Cater and colleagues showed that hippocampal cell death is independent of strain rate, suggesting that such rate dependence is not universal, or the sensitivity lies outside the experimental range.[33]

We tested Ca^{2+} responses to strain rate using high shear, 23 dyn/cm^2, and 10-ms pulse width with rise times of 2, 20, and 200 ms. Stimuli were set so that the *mean* shear stress over the stimuli was constant. Responses differed drastically between rapid and slow rise times. With a rise time of 2 ms, cells showed a significant Ca^{2+} increase (Fig. 3A), peaking in ~16 s (Fig. 3D, black curve). Response decreased with slower rise times (Fig. 3B,C). Peak calcium dropped from 220% with rise time of 2 ms to ~3% with rise time of 200 ms of the same amplitude (Fig. 3D). Maximum sensitivity to strain rate was obtained for rise times lower than 20 ms and reached steady state at 200 ms. Clearly, there is an effective dashpot in series with the Ca^{2+} influx pathway(s).

Ca^{2+} response to repeated shear pulses

To determine whether cells have a memory of the previous events, we applied repetitive stimuli. The pulse train contained low-amplitude pulses of 11.5 dyn/cm^2, with a rise time of 2 ms and duration of 10 ms that alone were not able to produce a Ca^{2+} rise (Fig. 2D). Each pulse train consisted of 10 pulses, separated by 10, 100, 1000, and 10,000 ms. Typical Ca^{2+} responses to a pulse train with 1-sec intervals is shown in Figure 4A. Individual cells were activated at different times with this train. At this frequency, ~20% of cells responded after the second pulse, whereas a majority of cells (60%) responded to the sixth and later pulses. This finding shows that the mechanical effect is cumulative, so the internal stresses take a measurable time to relax. The frequency of the pulse train plays an important role. With short intervals of 10 ms, the pulse train caused a 340% increase of Ca^{2+}, a response 4 times higher than a single pulse of the same amplitude with the same total duration of 100 ms (Fig. 4C). This suggests that an abrupt mechanical shock imposes a more activating effect than a sustained lower shear force, consistent with our observations from rise time studies (Fig. 3). This emphasizes the viscoelastic/plastic nature of the transduction process. At an interval of 10 sec, a time in which most of Ca^{2+} peaks would have fallen to the baseline, cells failed to respond with up to 10 consecutive pulses (Fig. 4B). Cells showed similar responses to a single pulse at low amplitude. Figure 4D shows peak Ca^{2+} with 10 consecutive pulses of various intervals, where we estimate the relaxation time to be ~100 ms.

We conducted finite element analysis on a hyperviscoelastic cell model,[34,35] and it showed that a shear pulse of 20 dyn/cm^2 and 10-ms width produced a maximum strain of 16%, followed by an oscillatory decay with relaxation time of ~100 ms (Supplementary Materials S2) (see online supplementary material at http://www.liebertpub.com), consistent with our experimental observations.

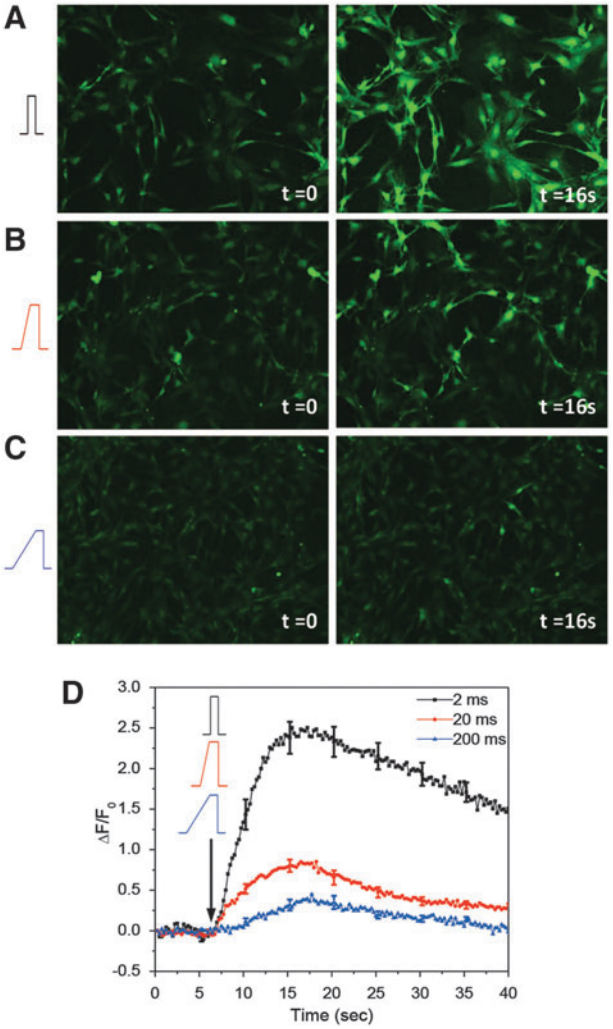

FIG. 3. Ca^{2+} responses to shear pulses of different rise times. (**A–C**) Images of Fluo-4-loaded astrocytes before ($t = 0$) and after ($t = 16$ sec) a shear stimulus (11.5 dyn/cm^2, 10 ms) with rise times of 2 (A), 20 (B), and 200 ms (C). (**D**) Changes in Ca^{2+} intensity averaged over 30 cells from four experiments for each condition, showing that high strain rate (2-ms rise time) produces larger response, whereas the response is drastically reduced when the rise time is longer than 20 ms. Scale bar is 100 μm. Color image is available online at www.liebertpub.com/neu

The response involves both Ca^{2+} influx and internal store release

It is postulated that the force-induced Ca^{2+} influx involves cationic MSCs[14–16] because the Ca^{2+} influx can be triggered by many mechanical stimuli, including fluid shear stress,[36] osmotic swelling,[37] and stretching.[18] The influx alone appears insufficient to account for the peak levels of Ca^{2+} given that the response is reduced in the presence of thapsigargin (Tg), suggesting a correlated Ca^{2+} release from internal stores.[38] To determine whether the Ca^{2+} influx was through known mechanosensitive ion channels, we tried Gd^{3+}, a nonspecific MSC blocker, and GsMTx4, a specific

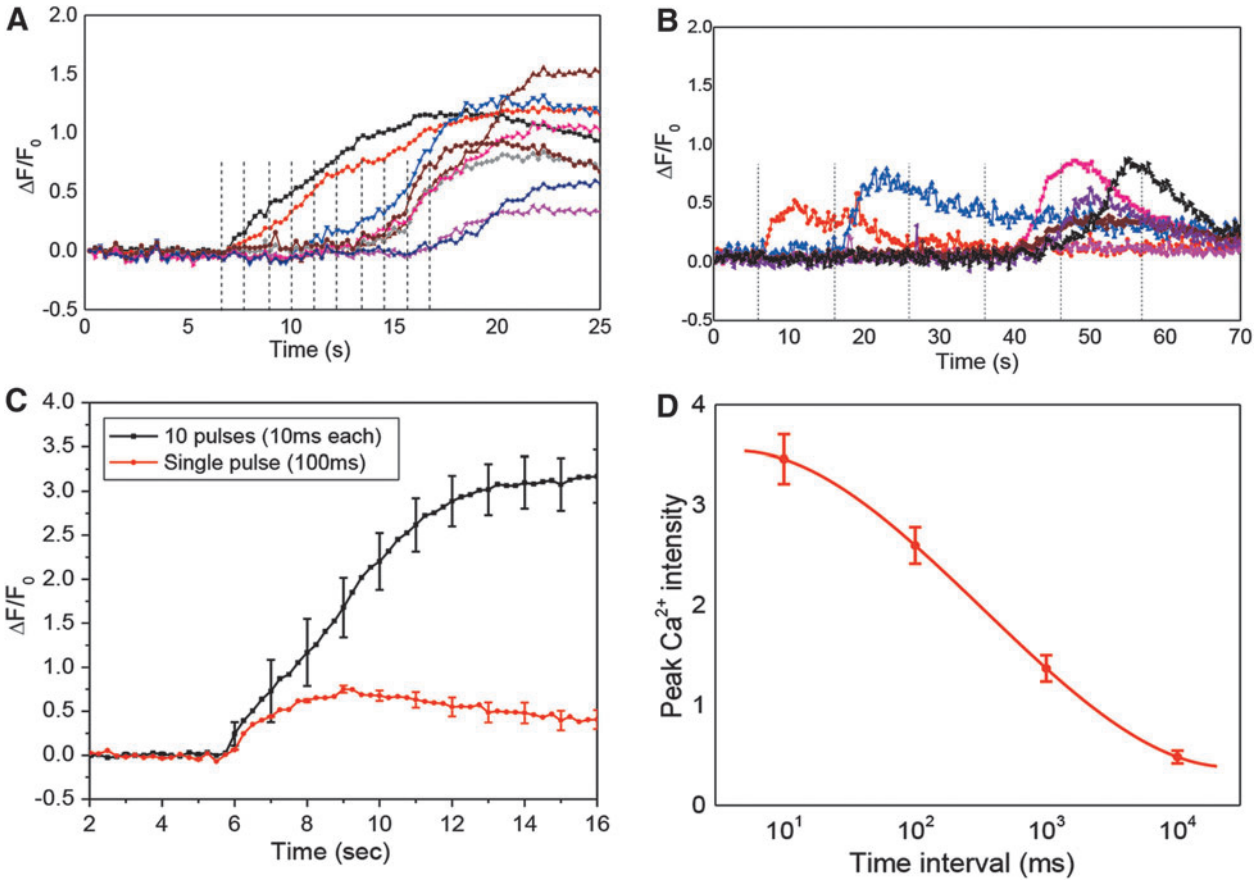

FIG. 4. Ca^{2+} responses to repeated shear pulses. (**A** and **B**) Ca^{2+} responses to a train of 10 narrow pulses of 11.5 dyn/cm^2 and 10-ms duration with rest intervals of 1 (A) and 10 sec (B). Dashed lines indicate the times when a pulse arrived. Note that cells can be activated by the subsequent pulses as shown in (A) and (B). (**C**) Comparison of Ca^{2+} responses to a train of 10 pulses of 11.5 dyn/cm^2 and 10 ms wide, and a single pulse of the same amplitude and 100 ms wide, showing that abrupt shear force imposes more response to a sustained force. Each curve was averaged from 30 cells in four experiments. (**D**) Average peak Ca^{2+} intensity triggered by pulse trains of different time intervals ($n = 30$) showing a relaxation time at $\sim$ 100 ms. Error bars indicate standard error of the mean. Color image is available online at www.liebertpub.com/neu

inhibitor for MSCs.[14] Cells treated with 100 μM of Gd^{3+} or in Ca^{2+}-free solution did not respond to the acute shear stimulus (23 dyn/cm^2 for 10 ms; $n = 30$; Fig. 5A). Disappointingly, 5 μM of GsMTx4 showed no significant inhibition, suggesting that there are other pathways for mechanically induced Ca^{2+} influx in astrocytes (Fig. 5A). Although there are MSCs that are sensitive to GsMTx4 in astrocytes,[32,39] we have previously shown that there are multiple MSCs in cells, and swelling-induced Ca^{2+} entry is not sensitive to GsMTx4 in astrocytes.[40] Shear responses were totally inhibited when extracellular calcium was removed and recovered after restoring calcium (Fig. 5B). These results consistently show that shear stress induces Ca^{2+} influx through currently undefined pathways.

To check on the role of Ca^{2+} stores, we depleted the stores with 5 μM of Tg before stimulation. Tg reduced the amplitude of the Ca^{2+} elevation, suggesting that both Ca^{2+} influx and store release contribute to response to shear stimulus. To estimate the role of each component, we treated cells with Tg (5 μM) to near total depletion, then applied the shear pulse. A superthreshold shear stimulus caused a transient Ca^{2+} peak (that fell within 60 sec) on top of the Tg-induced Ca^{2+} plateau (Fig. 5C). The ratio of the influx peak to the height of Tg-induced Ca^{2+} release was near 1:1, and the total Ca^{2+} level with shear (integrated over background) was comparable to controls under the same stimulation (Fig. 2C), showing that the transient Ca^{2+} influx contributed $\sim$50% of the response. The Ca^{2+} increase, not surprisingly, had two components; the first peak occurred immediately poststimulation as a result of the influx of Ca^{2+} and slowly inactivated (or desensitized) over $\sim$60 sec; the second peak (in many cases, a shoulder of the first peak) was mainly from the release of Ca^{2+} from intracellular stores.

Discussion

Our results show that there is a threshold shear stress ($\sim$11.5 dyn/cm^2 for 10 ms) for Ca^{2+} activation in cultured astrocytes (Fig. 2F). Although the magnitude of the shear forces is the dominant parameter of the stimulus, there are finite relaxation times present so that changes in stimulus duration or rise time can lead to a response from subthreshold stimuli. A complex map of thresholds containing amplitude and duration is shown in Figure 2H. The significance of each stimulus property was evaluated by fitting the profile of Ca^{2+} response with a two-state Boltzmann equation (Equation 1).

The force loading kinetics (rise time of the pulse) plays an essential role in Ca^{2+} response. This is evidenced by two experiments: First, an abrupt increase in force caused the Ca^{2+} rise, but a slow increase to the same amplitude failed to activate the cells (Fig. 3D). Second, Ca^{2+} intensity after 10 narrow pulses is 4 times the

intensity for one pulse of the same total duration (Fig. 4C). These results demonstrate that the cell's response to mechanical inputs is highly nonlinear, and the viscoelastic/plastic nature of cells plays a role in the activation of the mechanosensitive Ca^{2+} pathway. Cells withstand mechanical loading through support from cytoskeleton, a heterogeneous, anisotropic collection of dynamically cross-linked structural proteins.[41–45] The deformation of a cell depends on the intrinsic elastic deformation of fibrous cytoskeletal proteins and plastic deformation involving dynamics of reversible cross-linking and cytoskeleton reorganization.[46,47] Slow shear loading engages the plastic processes that significantly modify the local force around the Ca^{2+} transducers acting like dashpots in series with the transducer. The strain-rate dependence of cell injury has been observed in 3D matrix cultured neurons and astrocytes, showing an increase in membrane permeability to small molecules and an increase in post-insult cell death.[24,29] However, this effect was not observed in hippocampal tissues under biaxial stretch at strain rates ranging from 0.1 to 50 s^{-1},[33] and we have showed that dye leakage in stretched dystrophic myocytes could be inhibited by GsMTx4, suggesting that the membrane breakdown was secondary to the applied stress.[48] Different cell types have different properties, which is not surprising.[49] Our results show that the sensitivity to strain rate decays rapidly with the increase of rise time. The strain rate used in Cater and colleagues is in the range of 0.1–50 s^{-1}, corresponding to the rise times ranging from 20 to 10,000 ms, which is much longer than our rise times (2–200 ms; Fig. 3D).

Cells become more susceptible to shear force when subjected to multiple subthreshold challenges of short interval. The data suggest that cells possess slow relaxation rates with an effective memory time of ~10 sec (Fig. 4D). Although cytoplasmic solution viscosity may participate, it is more likely that the slow responses are due to cytoskeletal bonds breaking and reforming. The dynamic deformation of the cells was evaluated using a finite element model considering cells as hyper-viscoelastic material. The model shows that the maximum deformation occurs at the end of the pressure pulse suggesting that the cells do not use a fast adaptation system (Supplementary Materials S2) (see online supplementary material at http://www.liebertpub.com). The oscillatory relaxation of the cell has a time constant of ~100 ms, which is consistent with our experimental results. Strain distribution clearly varies with space, time, and stimulus properties. This knowledge of the critical stimulus parameters may allow improvement of protective helmets.

It has been postulated that the force-induced Ca^{2+} entry is through mechanosensitive pathways, including cationic MSCs and hemichannels, followed by a release of Ca^{2+} from intracellular stores.[14–16,50] In astrocytes, injury-induced Ca^{2+} elevation has been studied using a stretching model and Ca^{2+} variations have been reported to last for minutes to hours.[18,19] We do not know the messenger pathways and effectors that are modulating this response at these slow time scales. Further, different stimuli—stretching or fluid shear—may change severity and types of injury.

Fast, controllable shear stimuli allowed us to resolve initial triggering mechanisms and assay subsequent responses. Our results

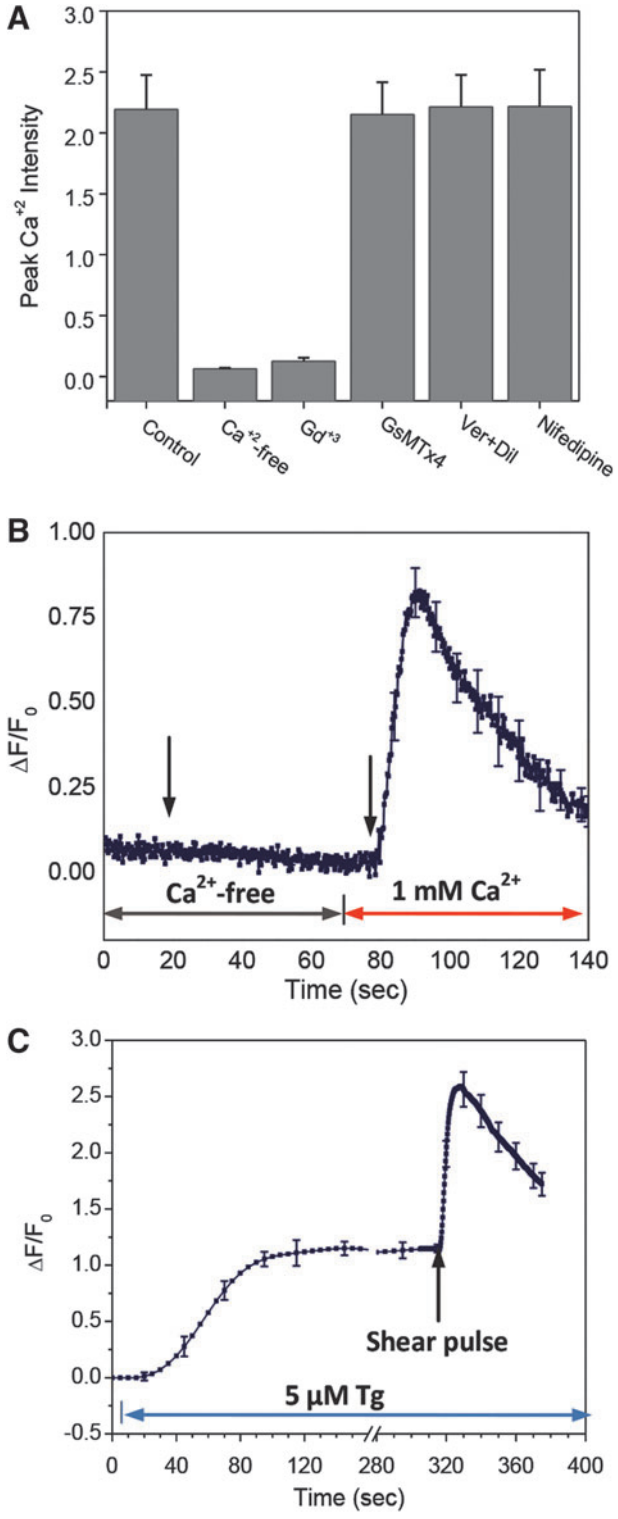

FIG. 5. Effect of inhibitors on shear induced Ca^{2+} response. (**A**) Peak Ca^{2+} intensity in control, Ca^{2+}-free, 10 μM Gd^{3+}, 5 μM GsMTx4, 10 μM verapamil and 10 μM nifedipine solution. A shear pulse of 23 dyn/cm^2 and 10 ms duration and 2 ms rise time was used for all experiments. The means are from n = 30 cells from four experiments under each condition. (**B**) Ca^{2+} response to the same shear pulse in Ca^{2+}-free solution, followed by the second pulse after adding 1 mM Ca^{2+} to the solution. The curve is averaged over 30 cells in 3 experiments. (**C**) Ca^{2+} response to 5 μM Tg. A shear stimulus was applied after the intensity reached a plateau, showing that the stimulus was able to induce significant Ca^{2+} influx after release of Ca^{2+} stores. The curve is averaged over 30 cells from 3 experiments of identical conditions. Error bars indicate standard error of the mean. Color image is available online at www.liebertpub.com/neu

show the existence of a two-step process: a primary calcium entry causing a transient Ca^{2+} peak and a Ca^{2+} release that lasts for longer times (Fig. 2C). Ca^{2+} response is clearly initiated by a Ca^{2+} influx through pathways that have yet to be defined. The response can be blocked completely by Gd^{3+}, a general inhibitor of many MSCs[51] and a modulator of bilayer structure (Fig. 5).[52,53] We have shown previously that MSCs of different types exist in astrocytes, and different MSCs can be used by cells to deal with different stimuli.[40] In astrocytes, cation currents activated by pressure applied to a patch can be blocked by GsMTx4, a known inhibitor specific to cationic MSCs,[54] whereas Ca^{2+} influx activated by swelling cannot be blocked.[40] The insensitivity to GsMTx4 of both shear-induced Ca^{2+} response and anisotonic stimulation suggests that they may have a common pathway. The insensitivity to various voltage-gated channel blockers shows that those channels are not involved in shear stimulation of Ca^{2+} influx in astrocytes.

The Ca^{2+} induced Ca^{2+} release from intracellular stores was common in our experiments, where the two peaks (Ca^{2+} entry and Ca^{2+} release) normally overlap. It has been shown that because of positive feedback, Ca^{2+} induced Ca^{2+} release appears as an ''all-or-none'' process where enough calcium is required to initiate the release of calcium from stores.[55–57] This suggests an alternative explanation for the extended Ca^{2+} peak. Under mild shear force, if a transient Ca^{2+} flux does not meet the threshold of Ca^{2+} store release level, it may not be able to activate the release. In this case, the accumulation of small amount of Ca^{2+} from subthreshold influxes can be integrated in the endoplasmic reticulum (ER) to later provide Ca^{2+} release supporting large changes in Ca^{2+}.

Despite these clear findings on the primary responses, the question arises as to why pathological responses can develop with such long delay times. After TBI stimuli, astrocytes swell[58,59] and undergo phenotypic changes with increased expression of glial-specific proteins, such as glial fibrillary acidic protein (GFAP).[60–62] The swelling appears within an hour after the stimulus.[63] Whereas it is generally believed that the swelling is associated with the accumulation of potassium ions and a reduction in extracellular sodium, calcium, and chloride,[58,64] most of the ion transport is through Ca^{2+}-dependent pathways. Thus, the early Ca^{2+} uptake may play a key role in cell volume and cell volume regulation. Our data suggest one or multiple mechanosensitive pathways may be accountable for Ca^{2+} uptake and volume regulation.[40] Possible candidates include transient receptor potential (TRP)V4[65] and/or TRPC1,[16] which are reported to respond to mechanical inputs in astrocytes. The phenotypic changes, that is, the formation of reactive astrogliosis through up-regulation of intermediate filament proteins such as GFAP, occur within a few hours of TBI.[66] Although the role of Ca^{2+} homeostasis in reactive astrogliosis is not clear, it has been shown that several Ca^{2+}-permeable channels, including TRPV4 and L-type Ca^{2+} channels, are up-regulated in reactive astrocytes.[65,67] A recent study showed that traumatic scratch injury to astrocytes triggers Ca^{2+} influx, resulting in an increase in GFAP expression and increase in the size of glial scars.[68] It suggests that Ca^{2+} provides the early injury signal that triggers the signal transduction cascades for astrogliosis through ER Ca^{2+} store release and this is consistent with our results. We provided direct evidence of such a Ca^{2+} pathway, and we further showed that activation of such Ca^{2+} responses is heterogeneous, depending on the stimulus properties.

Unlike *in vivo* models that measure the amplitude of total disrupting force and its duration and judge the injury by concussion or cell death,[13,69] our model has the ability to generate uniform and defined stimuli to a cell population and measure the earliest response before adaptation or inactivation sets in. However, the *in vitro* model has obvious deviations from *in vivo* conditions, including difference in extracellular matrix and local environments as well as lack of interaction with neurons and the chemical environment. We plan on extending the model by culturing the stimulated astrocytes for long times to see whether downstream damage occurs and under which stimulus conditions. If pathological responses do not happen, that may suggest that cellular interactions are necessary to create the pathology, and by coculturing neurons and astrocytes we can begin to address that issue.

Acknowledgments

This work was supported by National Institutes of Health (NIH) grant NS085517. The authors thank Dr. Paul Blank at the NIH for the encouragement and useful discussion at the beginning of the project.

Author Disclosure Statement

No competing financial interests exist.

References

1. Garman, R.H., Jenkins, L.W., Switzer, R.C., 3rd, Bauman, R.A., Tong, L.C., Swauger, P.V., Parks, S.A., Ritzel, D.V., Dixon, C.E., Clark, R.S., Bayir, H., Kagan, V., Jackson, E.K., and Kochanek, P.M. (2011). Blast exposure in rats with body shielding is characterized primarily by diffuse axonal injury. J. Neurotrauma 28, 947–959.
2. Sanborn, B., Nie, X., Chen, W., and Weerasooriya, T. (2012). Inertia effects on characterization of dynamic response of brain tissue. J. Biomech. 45, 434–439.
3. Chen, Y.C., Smith, D.H., and Meaney, D.F. (2009). In-vitro approaches for studying blast-induced traumatic brain injury. J. Neurotrauma 26, 861–876.
4. Maas, A.I., Stocchetti, N., and Bullock, R. (2008). Moderate and severe traumatic brain injury in adults. Lancet Neurol. 7, 728–741.
5. Young, J.A. (2012). Pharmacotherapy for traumatic brain injury: focus on sympathomimetics. Pharmacol. Ther. 134, 1–7.
6. North, S.H., Shriver-Lake, L.C., Taitt, C.R., and Ligler, F.S. (2012). Rapid analytical methods for on-site triage for traumatic brain injury. Annu. Rev. Anal. Chem. (Palo Alto Calif) 5, 35–56.
7. Koliatsos, V.E., Cernak, I., Xu, L., Song, Y., Savonenko, A., Crain, B.J., Eberhart, C.G., Frangakis, C.E., Melnikova, T., Kim, H., and Lee, D. (2011). A mouse model of blast injury to brain: initial pathological, neuropathological, and behavioral characterization. J. Neuropathol. Exp. Neurol. 70, 399–416.
8. Saljo, A., Svensson, B., Mayorga, M., Hamberger, A., and Bolouri, H. (2009). Low-level blasts raise intracranial pressure and impair cognitive function in rats. J. Neurotrauma 26, 1345–1352.
9. Kan, E.M., Ling, E.A., and Lu, J. (2012). Microenvironment changes in mild traumatic brain injury. Brain Res. Bull. 87, 359–372.
10. Chen, Y., and Swanson, R.A. (2003). Astrocytes and brain injury. J. Cereb. Blood Flow Metab. 23, 137–149.
11. Niggel, J., Sigurdson, W., and Sachs, F. (2000). Mechanically induced calcium movements in astrocytes, bovine aortic endothelial cells and C6 glioma cells. J. Membr. Biol. 174, 121–134.
12. Ostrow, L.W., and Sachs, F. (2005). Mechanosensation and endothelin in astrocytes—hypothetical roles in CNS pathophysiology. Brain Res. Brain Res. Rev. 48, 488–508.
13. Zhao, X., Ahram, A., Berman, R.F., Muizelaar, J.P., and Lyeth, B.G. (2003). Early loss of astrocytes after experimental traumatic brain injury. Glia 44, 140–152.
14. Suchyna, T.M., Tape, S.E., Koeppe, R.E., Andersen, O.S., Sachs, F., and Gottlieb, P.A. (2004). Bilayer-dependent inhibition of mechanosensitive channels by neuroactive peptide enantiomers. Nature 430, 235–240.
15. Ostrow, L.W., Suchyna, T.M., and Sachs, F. (2011). Stretch induced endothelin-1 secretion by adult rat astrocytes involves calcium influx via stretch-activated ion channels (SACs). Biochem. Biophys. Res. Commun. 410, 81–86.

16. Malarkey, E.B., Ni, Y., and Parpura, V. (2008). Ca^{2+} entry through TRPC1 channels contributes to intracellular Ca^{2+} dynamics and consequent glutamate release from rat astrocytes. Glia 56, 821–835.
17. Rzigalinski, B.A., Liang, S., McKinney, J.S., Willoughby, K.A., and Ellis, E.F. (1997). Effect of Ca^{2+} on in vitro astrocyte injury. J. Neurochem. 68, 289–296.
18. Rzigalinski, B.A., Weber, J.T., Willoughby, K.A., and Ellis, E.F. (1998). Intracellular free calcium dynamics in stretch-injured astrocytes. J. Neurochem. 70, 2377–2385.
19. Alford, P.W., Dabiri, B.E., Goss, J.A., Hemphill, M.A., Brigham, M.D., and Parker, K.K. (2011). Blast-induced phenotypic switching in cerebral vasospasm. Proc. Natl. Acad. Sci. U. S. A. 108, 12705–12710.
20. Weber, J.T., Rzigalinski, B.A., and Ellis, E.F. (2001). Traumatic injury of cortical neurons causes changes in intracellular calcium stores and capacitative calcium influx. J. Biol. Chem. 276, 1800–1807.
21. Chung, R.S., Staal, J.A., McCormack, G.H., Dickson, T.C., Cozens, M.A., Chuckowree, J.A., Quilty, M.C., and Vickers, J.C. (2005). Mild axonal stretch injury in vitro induces a progressive series of neurofilament alterations ultimately leading to delayed axotomy. J. Neurotrauma 22, 1081–1091.
22. Geddes-Klein, D.M., Schiffman, K.B., and Meaney, D.F. (2006). Mechanisms and consequences of neuronal stretch injury in vitro differ with the model of trauma. J. Neurotrauma 23, 193–204.
23. Ravin, R., Blank, P.S., Steinkamp, A., Rappaport, S.M., Ravin, N., Bezrukov, L., Guerrero-Cazares, H., Quinones-Hinojosa, A., Bezrukov, S.M., and Zimmerberg, J. (2012). Shear forces during blast, not abrupt changes in pressure alone, generate calcium activity in human brain cells. PLoS One 7, e39421.
24. Cullen, D.K., Vernekar, V.N., and LaPlaca, M.C. (2011). Trauma-induced plasmalemma disruptions in three-dimensional neural cultures are dependent on strain modality and rate. J. Neurotrauma 28, 2219–2233.
25. LaPlaca, M.C., Cullen, D.K., McLoughlin, J.J., and Cargill, R.S., 2nd. (2005). High rate shear strain of three-dimensional neural cell cultures: a new in vitro traumatic brain injury model. J. Biomech. 38, 1093–1105.
26. Besch, S.R., Suchyna, T., and Sachs, F. (2002). High-speed pressure clamp. Pflügers Arch. Eur. J. Phys. 445, 161–166.
27. Rahimzadeh, J., Meng, F., Sachs, F., Wang, J., Verma, D., and Hua, S.Z. (2011). Real-time observation of flow-induced cytoskeletal stress in living cells. Am. J. Physiol. Cell Physiol. 301, C646–C652.
28. Brode, H.L. (1959). Blast wave from a spherical charge. Phys. Fluids 2, 217–229.
29. Tamayol, A., and Bahrami, M. (2009). Analytical solutions for laminar fully-developed flow in microchannels with non-circular cross-section. Proceedings of the ASME Fluids Engineering Division Summer Meeting (FEDSM2009), August 2–5, Vail, Colorado.
30. Wang, J., Heo, J., and Hua, S.Z. (2010). Spatially resolved shear distribution in microfluidic chip for studying force transduction mechanisms in cells. Lab on a Chip 10, 235–239.
31. Liao, S.L., and Chen, C.J. (2001). Tyrosine kinase signaling involves in glutamate-induced astrocyte proliferation. Neuroreport 12, 3519–3522.
32. Ostrow, K.L., Mammoser, A., Suchyna, T., Sachs, F., Oswald, R., Kubo, S., Chino, N., and Gottlieb, P.A. (2003). cDNA sequence and in vitro folding of GsMTx4, a specific peptide inhibitor of mechanosensitive channels. Toxicon 42, 263–274.
33. Cater, H.L., Sundstrom, L.E., and Morrison, B., 3rd. (2006). Temporal development of hippocampal cell death is dependent on tissue strain but not strain rate. J. Biomech. 39, 2810–2818.
34. Gu, L.X., Chafi, M.S., Ganpule, S., and Chandra, N. (2012). The influence of heterogeneous meninges on the brain mechanics under primary blast loading. Compos. Part B Eng. 43, 3160–3166.
35. Rashid, B., Destrade, M., and Gilchrist, M.D. (2012). Mechanical characterization of brain tissue in compression at dynamic strain rates. J. Mech. Behav. Biomed. 10, 23–38.
36. Jensen, M.E., Odgaard, E., Christensen, M.H., Praetorius, H.A., and Leipziger, J. (2007). Flow-induced [Ca2+]i increase depends on nucleotide release and subsequent purinergic signaling in the intact nephron. J. Am. Soc. Nephrol. 18, 2062–2070.
37. Haeberle, H., Bryan, L.A., Vadakkan, T.J., Dickinson, M.E., and Lumpkin, E.A. (2008). Swelling-activated Ca^{2+} channels trigger Ca^{2+} signals in Merkel cells. PLoS One 3, e1750.
38. Verkhratsky, A., and Kettenmann, H. (1996). Calcium signalling in glial cells. Trends Neurosci. 19, 346–352.
39. Bowman, C.L., Gottlieb, P.A., Suchyna, T.M., Murphy, Y.K., and Sachs, F. (2007). Mechanosensitive ion channels and the peptide inhibitor GsMTx-4: history, properties, mechanisms and pharmacology. Toxicon 49, 249–270.
40. Hua, S.Z., Gottlieb, P.A., Heo, J., and Sachs, F. (2010). A mechanosensitive ion channel regulating cell volume. Am. J. Physiol. Cell Physiol. 298, C1424–C1430.
41. Verma, D., Ye, N.N., Meng, F.J., Sachs, F., Rahimzadeh, J., and Hua, S.Z. (2012). Interplay between cytoskeletal stresses and cell adaptation under chronic flow. PLoS One 7, e44167.
42. Meng, F., and Sachs, F. (2011). An orientation-based FRET sensor for real-time imaging of cellular forces. J. Cell Sci. 125, 743–750.
43. Meng, F., and Sachs, F. (2011). Measuring strain of structural proteins in vivo in real time, in: *Cardiac Mechano-Electric Coupling and Arrhythmia: From Pipette to Patient*. P. Kohl, F. Sachs, and M.R. Franz (eds). Oxford University Press: Oxford, UK, pps. 431–434.
44. Meng, F.J., and Sachs, F. (2011). Visualizing dynamic cytoplasmic forces with a compliance-matched FRET sensor. J.Cell Sci. 124, 261–269.
45. Rahimzadeh, J., Meng, F., Sachs, F., Wang, J., Verma, D., and Hua, S.Z. (2011). Real-time observation of flow-induced cytoskeletal stress in living cells. Am. J. Physiol. Cell Physiol. 301, C646–C652.
46. Gardel, M.L., Shin, J.H., MacKintosh, F.C., Mahadevan, L., Matsudaira, P., and Weitz, D.A. (2004). Elastic behavior of cross-linked and bundled actin networks. Science (New York, NY) 304, 1301–1305.
47. Bursac, P., Lenormand, G., Fabry, B., Oliver, M., Weitz, D.A., Viasnoff, V., Butler, J.P., and Fredberg, J.J. (2005). Cytoskeletal remodelling and slow dynamics in the living cell. Nat. Mater. 4, 557–561.
48. Yeung, E.W., Whitehead, N.P., Suchyna, T.M., Gottlieb, P.A., Sachs, F., and Allen, D.G. (2005). Effects of stretch-activated channel blockers on [Ca2+]i and muscle damage in the mdx mouse. J. Physiol. 562, 367–380.
49. Wang, Y., Meng, F., and Sachs, F. (2011). Genetically encoded force sensors for measuring mechanical forces in proteins. Commun. Integr. Biol. 4, 385–390.
50. De Bock, M., Decrock, E., Wang, N., Bol, M., Vinken, M., Bultynck, G., and Leybaert, L. (2014). The dual face of connexin-based astroglial Ca communication: a key player in brain physiology and a prime target in pathology. Biochim. Biophys. Acta 1843, 2211–2232.
51. Caldwell, R.A., Clemo, H.F., and Baumgarten, C.M. (1998). Using gadolinium to identify stretch-activated channels: technical considerations. Am. J. Physiol. 275, C619–C621.
52. Ermakov, Y.A., Averbakh, A.Z., Yusipovich, A.I., and Sukharev, S. (2001). Dipole potentials indicate restructuring of the membrane interface induced by gadolinium and beryllium ions. Biophys. J. 80, 1851–1862.
53. Ermakov, Y., Averbakh, A.Z., and Sukharev, S.I. (1997). Lipid and cell membranes in the presence of gadolinium and other ions with high affinity to lipids. 1. Dipole and diffuse components of the boundary potential. Membr. Cell Biol. 11, 539–554.
54. Suchyna, T.M., Markin, V.S., and Sachs, F. (2009). Biophysics and structure of the patch and the gigaseal. Biophys. J. 97, 738–747.
55. Usachev, Y.M., and Thayer, S.A. (1997). All-or-none Ca^{2+} release from intracellular stores triggered by Ca^{2+} influx through voltage-gated Ca^{2+} channels in rat sensory neurons. J. Neurosci. 17, 7404–7414.
56. Verkhratsky, A., and Shmigol, A. (1996). Calcium-induced calcium release in neurones. Cell Calcium 19, 1–14.
57. Jackson, J.G., and Thayer, S.A. (2006). Mitochondrial modulation of Ca^{2+}-induced Ca^{2+}-release in rat sensory neurons. J. Neurophysiol. 96, 1093–1104.
58. Kimelberg, H.K. (1992). Astrocytic edema in CNS trauma. J. Neurotrauma 9, Suppl. 1, S71–S81.
59. Reinert, M., Khaldi, A., Zauner, A., Doppenberg, E., Choi, S., and Bullock, R. (2000). High extracellular potassium and its correlates after severe head injury: relationship to high intracranial pressure. Neurosurg. Focus 8, e10.
60. Myer, D.J., Gurkoff, G.G., Lee, S.M., Hovda, D.A., and Sofroniew, M.V. (2006). Essential protective roles of reactive astrocytes in traumatic brain injury. Brain 129, 2761–2772.
61. Laird, M.D., Vender, J.R., and Dhandapani, K.M. (2008). Opposing roles for reactive astrocytes following traumatic brain injury. Neurosignals 16, 154–164.

62. Wilhelmsson, U., Bushong, E.A., Price, D.L., Smarr, B.L., Phung, V., Terada, M., Ellisman, M.H., and Pekny, M. (2006). Redefining the concept of reactive astrocytes as cells that remain within their unique domains upon reaction to injury. Proc. Natl. Acad. Sci. U. S. A. 103, 17513–17518.
63. Dietrich, W.D., Alonso, O., and Halley, M. (1994). Early microvascular and neuronal consequences of traumatic brain injury: a light and electron microscopic study in rats. J. Neurotrauma 11, 289–301.
64. Kimelberg, H.K., Rutledge, E., Goderie, S., and Charniga, C. (1995). Astrocytic swelling due to hypotonic or high K+ medium causes inhibition of glutamate and aspartate uptake and increases their release. J. Cereb. Blood Flow Metab. 15, 409–416.
65. Butenko, O., Dzamba, D., Benesova, J., Honsa, P., Benfenati, V., Rusnakova, V., Ferroni, S., and Anderova, M. (2012). The increased activity of TRPV4 channel in the astrocytes of the adult rat hippocampus after cerebral hypoxia/ischemia. PLoS One 7, e39959.
66. Pekny, M., and Nilsson, M. (2005). Astrocyte activation and reactive gliosis. Glia 50, 427–434.
67. Daschil, N., Obermair, G.J., Flucher, B.E., Stefanova, N., Hutter-Paier, B., Windisch, M., Humpel, C., and Marksteiner, J. (2013). CaV1.2 calcium channel expression in reactive astrocytes is associated with the formation of amyloid-beta plaques in an Alzheimer's disease mouse model. J. Alzheimers Dis. 37, 439–451.
68. Gao, K., Wang, C.R., Jiang, F., Wong, A.Y., Su, N., Jiang, J.H., Chai, R.C., Vatcher, G., Teng, J., Chen, J., Jiang, Y.W., and Yu, A.C. (2013). Traumatic scratch injury in astrocytes triggers calcium influx to activate the JNK/c-Jun/AP-1 pathway and switch on GFAP expression. Glia 61, 2063–2077.
69. Greenwald, R.M., Gwin, J.T., Chu, J.J., and Crisco, J.J. (2008). Head impact severity measures for evaluating mild traumatic brain injury risk exposure. Neurosurgery 62, 789–798; discussion, 798.

Address correspondence to:
Susan Z. Hua, PhD
Department of Mechanical and Aerospace Engineering
SUNY-Buffalo
340 Jarvis Hall
Buffalo, NY 14260

E-mail: zhua@buffalo.edu